

# Approximate N<sup>2</sup>LO and N<sup>3</sup>LO QCD Predictions for $tW$ Production

Jia-Le Ding,<sup>1,\*</sup> Hai Tao Li,<sup>1,†</sup> and Jian Wang<sup>1,2,‡</sup>

<sup>1</sup>*School of Physics, Shandong University, Jinan, Shandong 250100, China*

<sup>2</sup>*Center for High Energy Physics, Peking University, Beijing 100871, China*

We report a calculation of approximate next-to-next-to-leading-order (N<sup>2</sup>LO) and next-to-N<sup>2</sup>LO (N<sup>3</sup>LO) QCD corrections to associated  $tW$  production at the LHC, which constitute the dominant contributions to full perturbative predictions. The approximate N<sup>2</sup>LO corrections consist of the large logarithmic terms  $\ln^n(1 - Q^2/\hat{s})$  (with  $\sqrt{\hat{s}}$  being the partonic center-of-mass energy and  $Q$  the invariant mass of the  $tW$  system) and the terms proportional to  $\delta(1 - Q^2/\hat{s})$  at  $\mathcal{O}(\alpha_s^2)$ , which are obtained by utilizing the newly obtained two-loop hard and soft functions. The approximate N<sup>3</sup>LO corrections further include the large logarithms at  $\mathcal{O}(\alpha_s^3)$  by using renormalization group evolution equations and the three-loop soft anomalous dimension, while the  $\delta(1 - Q^2/\hat{s})$  term is only partially accurate at this order. Numerical evaluation reveals that they increase the NLO cross section by more than 10%. The inclusion of these higher-order corrections leads to improved agreement with the experimental data at the LHC, resulting in a direct determination of the CKM matrix element  $|V_{tb}| = 0.99 \pm 0.03(\text{exp.}) \pm 0.03(\text{theo.})$  without assuming unitarity of the matrix.

## I. INTRODUCTION

Single top-quark production at the Large Hadron Collider (LHC) provides a probe of the  $tWb$  vertex and hence of the electroweak coupling of the top quark. There are three phenomenologically distinct production channels. The  $s$ -channel involves a time-like  $W$  boson and produces the top quark together with a light antiquark. The  $t$ -channel is driven by the exchange of a space-like  $W$  boson between a light quark and the bottom quark. The cross sections of these two channels may be affected by effective four-quark operators [1, 2]. The  $tW$  associated production channel produces a top quark and a real  $W$  boson simultaneously and can probe the  $tWb$  coupling more directly. At the LHC, this channel has the second-largest cross section and serves as a significant background in many searches for new physics signals. Precise measurements of this process and detailed comparisons with theoretical predictions impose stringent tests of the Standard Model and may give a smoking-gun signal of new physics. Measurements of the total and differential  $tW$  cross sections have been reported by the ATLAS [3–7] and CMS collaborations [8–13].

On the theoretical side, the  $tW$  amplitude interferes with the  $t\bar{t}$  production beyond the leading order (LO) in QCD, which complicates the definition of the signal and increases theoretical uncertainties, posing interesting phenomenological challenges. To date, the most precise full fixed-order prediction for  $tW$  production is at next-to-leading order (NLO) in QCD [14–17]. NLO calculations matched to parton showers were performed in Refs. [18–20]. Higher-order effects from soft-gluon radiation have been studied in Refs. [21–25].

Because  $tW$  production interferes with  $t\bar{t}$  production

and the process contains massive color particles, the computation of N<sup>2</sup>LO QCD corrections is particularly challenging. In recent years, significant progress towards N<sup>2</sup>LO corrections has been achieved. The two-loop virtual corrections and the N<sup>2</sup>LO  $N$ -jettiness soft function have been computed in Refs. [26–31] and Refs. [32, 33], respectively. The problem of  $t\bar{t}$  interference in the one-loop (virtual-real) contributions was resolved in [34]. However, the interference in the double-real correction remains a challenge, and thus the full N<sup>2</sup>LO result is still unavailable. In this work, we provide approximate N<sup>2</sup>LO and N<sup>3</sup>LO, denoted by aN<sup>2</sup>LO and aN<sup>3</sup>LO, respectively, QCD predictions for  $tW$  production that are induced by virtual loops and soft radiations. These higher-order corrections are derived from the factorization property of the cross section near the threshold, i.e., it can be factorized as a convolution of a hard function, a soft function, and parton distribution functions (PDFs) [24]. The hard function describes the virtual loop effects and has been computed up to N<sup>2</sup>LO in analytical and numerical form for the leading color [30] and full result [31], respectively. The soft function encompasses all the effects of soft radiations and has also been calculated at N<sup>2</sup>LO in our previous work [35]. In addition, by using the three-loop anomalous dimensions for the renormalization group (RG) evolution of the hard and soft functions [36], we can even derive all the large logarithmic (scale-dependent) terms up to N<sup>3</sup>LO. As will be shown in the numerical discussion, these approximate predictions provide dominant contributions to the full results.

We note that the aN<sup>2</sup>LO and aN<sup>3</sup>LO cross sections were investigated based on the traditional resummation formalism [22, 23, 25, 37, 38]. However, the threshold variable is defined differently, which will be shown explicitly in the next section, and the N<sup>2</sup>LO scale-independent parts of the hard and soft functions are not included. Moreover, the formalism in Ref. [25] employs the three-loop soft anomalous dimensions [38] that do not take into account the tripole correlation involving one massive and two massless partons. Our improvements in the

\* dingjl@mail.sdu.edu.cn

† haitao.li@sdu.edu.cn

‡ j.wang@sdu.edu.cn

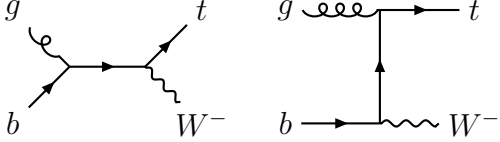


FIG. 1: LO Feynman diagrams for  $tW^-$  production.

higher-order hard/soft functions and anomalous dimensions enable us to obtain the most advanced prediction for this important process. The numerical results in this work reveal that higher-order QCD corrections beyond NLO increase the cross section obviously, leading to improved agreement between theoretical predictions and experimental measurements.

This paper is organized as follows. In Sec. II, we present the factorization formula and discuss the logarithmic structure of the threshold expansion. Sec. III contains our numerical results and phenomenological discussion. We summarize in Sec. IV, and collect useful expressions for the anomalous dimensions in Appendix A.

## II. FACTORIZATION FORMALISM

We consider the associated top quark and  $W$  boson production at the LHC, i.e.,  $p(P_1) + p(P_2) \rightarrow t/\bar{t}(p_3) + W^-/W^+(p_4) + X(p_X)$ , where  $X$  accounts for all additional radiation in the final state. This process is characterized by the Lorentz invariant kinematic variables,  $s = (P_1 + P_2)^2$ ,  $Q^2 = (p_3 + p_4)^2$ , which define the ratio  $\tau = Q^2/s$ . In the hadronic threshold limit,  $1 - \tau \rightarrow 0$ , only soft parton radiation is allowed in  $X$ . The soft radiation induces large logarithmic terms in the cross section, which dominate higher-order QCD corrections. For comparison, the threshold variable in Refs. [22, 23, 25, 37, 38] is defined by  $S_4 = 2p_4 \cdot p_X$ , which measures the soft limit in a different way.

The corresponding LO partonic scattering process is  $b/\bar{b}(p_1) + g(p_2) \rightarrow t/\bar{t}(p_3) + W^-/W^+(p_4)$  with the LO Feynman diagrams shown in Fig. 1. The partonic center-of-mass energy  $\sqrt{s}$  is defined by  $\hat{s} = (p_1 + p_2)^2$ , which can be used to define the variable  $z = Q^2/\hat{s}$ . The partonic threshold is described by  $\bar{z} = 1 - z \rightarrow 0$ .

In the threshold limit, the differential hadronic cross section can be expressed in a factorization form [24]

$$\frac{d\sigma}{dQ^2 d\Phi_2} = \frac{1}{s} \int_{\tau}^1 \frac{dz}{z} \mathcal{L} \left( \frac{\tau}{z}, \mu \right) \frac{1}{2Q^2} H(\mu, \beta_t, y) \times \mathcal{S}(\bar{z}, \mu, \beta_t, y), \quad (1)$$

where  $\Phi_2$  denotes the two-body phase space, and the parton luminosity  $\mathcal{L}$  is defined as the convolution

$$\mathcal{L} \left( \frac{\tau}{z}, \mu \right) = \int_{\tau/z}^1 \frac{dx}{x} \left[ f_b(x, \mu) f_g \left( \frac{\tau}{xz}, \mu \right) + (b \leftrightarrow g) \right]$$

with  $f_{b/g}(x, \mu)$  being the PDF at the scale  $\mu$ . The PDF is strongly suppressed in the region  $x \rightarrow 1$ . Therefore, the parton luminosity turns out to have a larger value as  $z \rightarrow 1$ , i.e., the partonic threshold limit can be reached even if the hadronic limit  $\tau \rightarrow 1$  is not fully realized [39]. The hard function  $H$  is process-dependent and can be obtained by calculating the corresponding virtual correction to the partonic scattering process. It is a function of  $y \equiv \cos \theta$  with  $\theta$  the polar angle of the outgoing top quark relative to the incoming bottom quark and the velocity of the top quark,  $\beta_t$ , which is defined by  $\beta_t = \sqrt{(Q^2 - m_t^2 - m_W^2)^2 - 4m_t^2 m_W^2}/(Q^2 + m_t^2 - m_W^2)$ . The soft function  $\mathcal{S}$  encodes the effects of soft radiations in terms of logarithms  $((\ln \bar{z})^{2n-i}/\bar{z})_+$  with  $i = 1, \dots, 2n$  at order  $\alpha_s^n$ . The subscript '+' indicates that the pole at  $z = 1$  is subtracted, e.g.,

$$\int_0^1 dz f(z) \left( \frac{\ln \bar{z}}{\bar{z}} \right)_+ = \int_0^1 dz [f(z) - f(1)] \frac{\ln \bar{z}}{\bar{z}}. \quad (2)$$

The resummed cross section in momentum space can be derived [24]

$$\frac{d\sigma}{dQ^2 d\Phi_2} = \frac{1}{s} \int_{\tau}^1 \frac{dz}{z} \mathcal{L} \left( \frac{\tau}{z}, \mu_f \right) \frac{1}{2Q^2} H(\mu_h, \beta_t, y) \times U_m(\mu_h, \mu_s, \mu_f) \frac{z^{-\eta}}{\bar{z}^{1-2\eta}} \tilde{\mathcal{S}} \left( \ln \frac{\bar{z}^2 Q^2}{z \mu_s^2} + \partial_{\eta}, \beta_t, y \right) \frac{e^{-2\gamma_E \eta}}{\Gamma(2\eta)} \quad (3)$$

where both the evolution factor  $U_m$  and  $\eta$  depend on the hard and soft scales,  $\mu_h$  and  $\mu_s$ . Their explicit form is not relevant if we only focus on the fixed-order expansion, in which all the scales are set equal. In this case,  $U_m = 1$  and  $\eta = 0$ . Notice that one has to apply the derivative with respect to  $\eta$  before setting  $\eta = 0$ . Recent advances have provided the necessary ingredients for high-precision predictions. The two-loop hard function  $H$  has been obtained in Refs. [30, 31], and the  $N^2$ LO soft function  $\tilde{\mathcal{S}}$  in the Laplace space was calculated in Ref. [35].

The  $aN^3LO$  results for hard and soft functions are obtained by solving the RG evolution equations. The RG evolution of the Laplace transformed soft function  $\tilde{\mathcal{S}}(t, \mu) \equiv \int_0^\infty d\bar{z} e^{-\bar{z}/t} \mathcal{S}(\bar{z}, \mu)$  reads

$$\frac{d\tilde{\mathcal{S}}(t, \mu)}{d \ln \mu} = \gamma_s \tilde{\mathcal{S}}(t, \mu), \quad (4)$$

where the soft anomalous dimension is given by

$$\begin{aligned} \gamma_s = & - \left( \mathbf{T}_1^2 + \mathbf{T}_2^2 \right) \gamma_{\text{cusp}} \ln \left( \frac{\hat{s}t^2}{\mu^2} \right) - 2\gamma_q - 2\gamma_g - 2\gamma_Q \\ & + \mathbf{T}_1 \cdot \mathbf{T}_3 \gamma_{\text{cusp}} \ln \frac{(1 - \beta_t y)^2}{1 - \beta_t^2} + \mathbf{T}_2 \cdot \mathbf{T}_3 \gamma_{\text{cusp}} \ln \frac{(1 + \beta_t y)^2}{1 - \beta_t^2} \\ & - 2\gamma_f^q - 2\gamma_f^g - 2\mathcal{T}_{1233} \left( \frac{\alpha_s}{4\pi} \right)^3 \mathcal{F}_{h2} \left( \frac{1 - \beta_t^2}{1 - \beta_t^2 y^2} \right). \end{aligned} \quad (5)$$

Here  $\mathbf{T}_i$  represents the color charge associating with the  $i$ -th parton [40, 41].  $\mathcal{T}_{1233}$  is a new color structure that first appears at three-loop order, defined as

$$\mathcal{T}_{1233} = \frac{1}{2} f^{ade} f^{bce} \mathbf{T}_1^a \mathbf{T}_2^b (\mathbf{T}_3^c \mathbf{T}_3^d + \mathbf{T}_3^d \mathbf{T}_3^c), \quad (6)$$

and for  $tW$  production  $\mathcal{T}_{1233}$  can be replaced by  $-3/4$ . The associating function  $\mathcal{F}_{h2}$  was calculated in [36]. The cusp  $\gamma_{\text{cusp}}$  and the other anomalous dimensions  $\gamma_q, \gamma_g, \gamma_Q$  have been obtained up to  $\text{N}^3\text{LO}$  [42–44].

The RG evolution of the Laplace transformed PDFs in the threshold limit can be found in Refs. [42, 45],

$$\frac{d\tilde{f}_i(t, \mu)}{d\ln\mu} = (2\mathbf{T}_i \cdot \mathbf{T}_i \gamma_{\text{cusp}} \ln t + 2\gamma_f^i) \tilde{f}_i(t, \mu). \quad (7)$$

The anomalous dimensions  $\gamma_f^i$  ( $i = q, g$ ) are well-known [39, 46].

The RG evolution of the hard function can be derived from the fact that the total physical cross section must be independent of the scale  $\mu$ . This scale independence condition is expressed as

$$\frac{d\ln H}{d\ln\mu} + \frac{d\ln\tilde{f}_q}{d\ln\mu} + \frac{d\ln\tilde{f}_g}{d\ln\mu} + \frac{d\ln\tilde{\mathcal{S}}}{d\ln\mu} = 0. \quad (8)$$

The explicit expressions for the required anomalous dimensions are collected in Appendix A.

The fixed-order partonic cross section in the threshold limit contains a series of logarithmically enhanced terms, which can be written as

$$\frac{d\hat{\sigma}}{dQ^2 d\Phi_2} = \frac{d\hat{\sigma}_{\text{LO}}}{dQ^2 d\Phi_2} \sum_{n=0} \left( \frac{\alpha_s(\mu_r)}{4\pi} \right)^n \left( \sum_{m=-1}^{2n-1} C_{n,m} P_m \right)$$

where  $P_m$  denotes the distribution  $\left[ \frac{1}{\bar{z}} \left( \ln \frac{\bar{z}^2 Q^2}{z \mu_f^2} \right)^m \right]_+$  for  $m \geq 0$  and  $\delta(1-z)$  for  $m = -1$ . The corresponding coefficients are given by

$$\begin{aligned} C_{n,2n-1} &= \frac{n}{4^{n-1} n!} (-\gamma_{s,d}^{(0)})^n, \\ C_{n,2n-2} &= -\frac{n(2n-1)}{4^{n-1} n!} (-\gamma_{s,d}^{(0)})^{n-1} \left[ \gamma_{s,c}^{(0)} + \frac{2(n-1)}{3} \beta_0 \right], \\ C_{1,-1} &= -\frac{1}{4} \ln^2 \frac{Q^2}{\mu_f^2} \left( \gamma_{h,d}^{(0)} + \gamma_{s,d}^{(0)} \right) - \frac{1}{2} \ln \frac{Q^2}{\mu_f^2} \left( \gamma_{h,c}^{(0)} + \gamma_{s,c}^{(0)} \right) \\ &\quad - \beta_0 \ln \frac{Q^2}{\mu_r^2} + H_c^{(1)} + \tilde{\mathcal{S}}_c^{(1)}, \\ C_{2,1} &= -\frac{\pi^2}{2} (\gamma_{s,d}^{(0)})^2 + \frac{1}{4} \left[ \ln^2 \frac{Q^2}{\mu_f^2} \gamma_{s,d}^{(0)} \gamma_{h,d}^{(0)} \right. \\ &\quad \left. + 2 \ln \frac{Q^2}{\mu_f^2} \gamma_{s,d}^{(0)} \left( \gamma_{h,c}^{(0)} - 2\beta_0 \right) + 8\beta_0 \ln \frac{Q^2}{\mu_r^2} \gamma_{s,d}^{(0)} \right. \\ &\quad \left. + 2\gamma_{s,c}^{(0)} \left( \gamma_{s,c}^{(0)} + 2\beta_0 \right) - 4\gamma_{s,d}^{(0)} \left( H_c^{(1)} + \tilde{\mathcal{S}}_c^{(1)} \right) - 4\gamma_{s,d}^{(1)} \right], \end{aligned}$$

$$\begin{aligned} C_{3,3} &= \frac{5\pi^2}{24} (\gamma_{s,d}^{(0)})^3 - \frac{\gamma_{s,d}^{(0)}}{48} \left[ 3 \ln^2 \frac{Q^2}{\mu_f^2} \gamma_{s,d}^{(0)} \gamma_{h,d}^{(0)} \right. \\ &\quad \left. + 6 \ln \frac{Q^2}{\mu_f^2} \gamma_{s,d}^{(0)} \left( \gamma_{h,c}^{(0)} - 4\beta_0 \right) + 36\beta_0 \ln \frac{Q^2}{\mu_r^2} \gamma_{s,d}^{(0)} \right. \\ &\quad \left. + 4\gamma_{s,c}^{(0)} \left( 3\gamma_{s,c}^{(0)} + 10\beta_0 \right) - 12\gamma_{s,d}^{(0)} \left( H_c^{(1)} + \tilde{\mathcal{S}}_c^{(1)} \right) \right] \end{aligned}$$

$$+ 16\beta_0^2 - 24\gamma_{s,d}^{(1)} \Big], \quad (9)$$

where the anomalous dimensions are defined by

$$\begin{aligned} \gamma_{s,d} &= -\gamma_{\text{cusp}} (C_A + C_F), \\ \gamma_{s,c} &= \gamma_{\text{cusp}} \left[ \frac{C_A - 2C_F}{2} \ln \frac{(1 - \beta_t y)^2}{1 - \beta_t^2} - \frac{C_A}{2} \ln \frac{(1 + \beta_t y)^2}{1 - \beta_t^2} \right. \\ &\quad \left. - 2\gamma_f^q - 2\gamma_f^g - 2\gamma_q - 2\gamma_g - 2\gamma_Q, \right] \\ \gamma_{h,d} &= \gamma_{\text{cusp}} (C_A + C_F), \\ \gamma_{h,c} &= \gamma_{\text{cusp}} \left[ \frac{C_A}{2} \ln \frac{(1 + \beta_t y)^2}{1 - \beta_t^2} - \frac{C_A - 2C_F}{2} \ln \frac{(1 - \beta_t y)^2}{1 - \beta_t^2} \right] \\ &\quad + 2\gamma_q + 2\gamma_g + 2\gamma_Q, \end{aligned} \quad (10)$$

and  $\beta_0 = 11C_A/3 - 4T_F n_f/3$  with  $n_f$  the number of massless quark flavors. We have used  $H_c$  and  $\tilde{\mathcal{S}}_c$  to represent the scale-independent parts of hard and soft functions, respectively. The quantities have been expanded in a series of  $\alpha_s/4\pi$ , e.g.,  $\gamma_{s,d} = \sum_{n=0} \left( \frac{\alpha_s}{4\pi} \right)^{n+1} \gamma_{s,d}^{(n)}$ .

In the above equations, we have presented the results for the leading logarithms explicitly. The other subleading logarithms are too lengthy to be shown here and can be found in the auxiliary file. All the above coefficients are exact except only for  $C_{3,-1}$  where the three-loop scale-independent parts of the hard and soft functions,  $H_c^{(3)}$  and  $\tilde{\mathcal{S}}_c^{(3)}$ , are still lacking.

The discerning reader may have noted that the renormalization and factorization scales,  $\mu_r$  and  $\mu_f$ , have been clearly distinguished. This is made possible by making use of the fact that the partonic cross section is independent of the renormalization scale order-by-order in  $\alpha_s$  and the dependence of  $\alpha_s(\mu_r)$  on  $\mu_r$  is predictable.

The above expression can be considered as the leading power (LP) expansion in  $\bar{z}$ , i.e., the  $\mathcal{O}(\bar{z}^{-1})$  contribution in the cross section, denoted by  $\text{N}^n\text{LO}_{\text{LP}}$ . The subleading power corrections consist of the higher power terms in the  $gb$  channel and the contribution of the other partonic channels, both of which are of  $\mathcal{O}(\bar{z}^i)$  with  $i \geq 0$ . These corrections do not have a general structure that can be predicted without a full calculation and also suffer from the complicated problem of interference with  $t\bar{t}$  production. We only include them in QCD NLO theoretical predictions and adopt the power subtraction to deal with the interference problem [34]. As such, the  $\text{aN}^n\text{LO}$  prediction of the cross section is defined as

$$d\sigma(\text{aN}^n\text{LO}) = d\sigma(\text{N}^n\text{LO}_{\text{LP}}) + d\sigma(\text{NLO}) - d\sigma(\text{NLO}_{\text{LP}}).$$

### III. NUMERICAL RESULTS

For the numerical evaluation, we take the electroweak input parameters,  $M_W = 80.369 \text{ GeV}$ ,  $G_F = 1.16639 \times 10^{-5} \text{ GeV}^{-2}$ ,  $m_t = 172.57 \text{ GeV}$ ,  $\alpha = 1/132.5$ . We utilize the PDF4LHC21 PDF sets [47] and the associated

$\sqrt{s}$	7 TeV	8 TeV	13 TeV	13.6 TeV	14 TeV
LO	$10.7^{+2.3}_{-1.8} \pm 0.3$	$15.4^{+3.2}_{-2.5} \pm 0.4$	$51.4^{+9.3}_{-7.3} \pm 1.1$	$57.1^{+10.2}_{-8.1} \pm 1.2$	$60.9^{+10.8}_{-8.6} \pm 1.2$
NLO	$14.6^{+0.4}_{-0.5} \pm 0.5$	$20.9^{+0.6}_{-0.7} \pm 0.7$	$68.7^{+2.5}_{-2.9} \pm 1.4$	$76.1^{+2.7}_{-3.2} \pm 1.5$	$81.3^{+2.8}_{-3.5} \pm 1.6$
$N^2LO_{LP}$	$18.5^{+0.6}_{-0.8} \pm 0.5$	$26.3^{+0.8}_{-1.0} \pm 0.7$	$84.8^{+2.3}_{-2.8} \pm 1.7$	$93.7^{+2.5}_{-3.1} \pm 1.8$	$99.9^{+2.6}_{-3.1} \pm 1.9$
$N^3LO_{LP}$	$19.1^{+0.2}_{-0.3} \pm 0.5$	$27.1^{+0.2}_{-0.4} \pm 0.6$	$86.8^{+0.5}_{-1.0} \pm 1.7$	$95.9^{+0.6}_{-1.1} \pm 1.9$	$102.2^{+0.6}_{-1.2} \pm 1.9$
$aN^2LO$	$16.6^{+0.4}_{-0.5} \pm 0.5$	$23.8^{+0.6}_{-0.7} \pm 0.6$	$77.2^{+1.8}_{-2.2} \pm 1.6$	$85.4^{+2.1}_{-2.5} \pm 1.7$	$91.2^{+2.1}_{-2.8} \pm 1.8$
$aN^3LO$	$17.2^{+0.8}_{-0.9} \pm 0.5$	$24.5^{+1.1}_{-1.3} \pm 0.7$	$79.2^{+3.5}_{-3.8} \pm 1.6$	$87.6^{+3.9}_{-4.2} \pm 1.7$	$93.5^{+4.1}_{-4.6} \pm 1.8$

TABLE I: The fixed-order predictions for total cross sections of  $tW^-/\bar{t}W^+$  production (in pb). The first and second errors represent the scale and PDF uncertainties, respectively. The NLO cross sections are calculated using the power subtraction scheme.

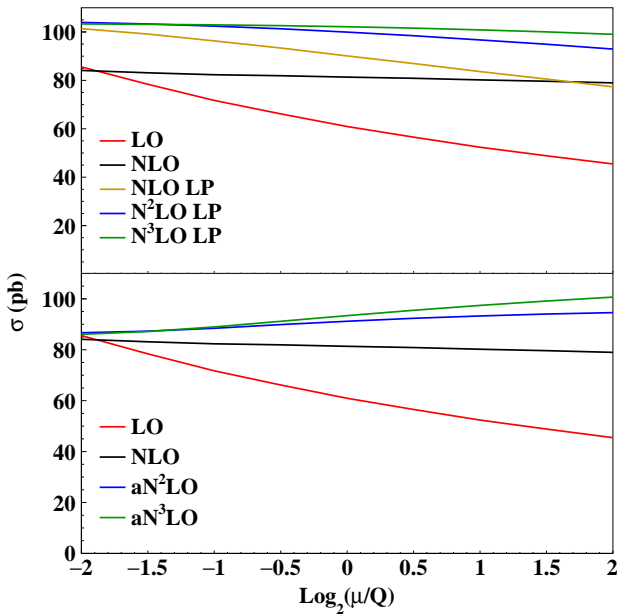


FIG. 2: Scale dependence of the inclusive  $tW^-/\bar{t}W^+$  cross section with  $\mu_r = \mu_f = \mu$  at the 14 TeV LHC. Both panels display exact LO (red) and NLO (black) results. The top panel also shows the LP predictions at  $NLO_{LP}$  (yellow),  $N^2LO_{LP}$  (blue) and  $N^3LO_{LP}$  (green). The bottom panel also shows the approximate  $N^2LO$  (blue) and  $N^3LO$  (green) results.

$\alpha_s(m_Z) = 0.118$  in the LHAPDF library [48]. The theoretical uncertainties of our predictions are estimated from two primary sources, i.e., the choice of unphysical scales and the PDFs. The scale uncertainty is estimated by varying the renormalization and factorization scales independently by a factor of two around their central value. The maximum and minimum values obtained from this nine-point variation define the upper and lower bounds. The PDF uncertainty is evaluated according to the symmetric Hessian prescription [47].

Fig. 2 presents the dependence of the inclusive cross section on the renormalization and factorization scales

with  $\mu_r = \mu_f = \mu$  at the 14 TeV LHC. As shown by the LP predictions in the top panel, including higher-order corrections significantly reduces the scale dependence. The NLO LP prediction is very close to the full NLO result. The two even coincide if the scale is chosen around  $3Q$ , indicating that higher-order corrections are dominated by the LP approximation. We also observe that the full NLO result exhibits a mild sensitivity to the scale variation. This is because the subleading power correction, albeit small in magnitude, has a strong scale dependence which varies precisely in an opposite way to that at LP. The bottom panel shows the approximate higher-order predictions, including subleading power corrections at NLO. The higher-order effects become more pronounced as the scale increases. The scale uncertainties would be further reduced after computing the full  $N^2LO$  QCD corrections.

In Tab. I, we present numerical results of the total cross sections and their scale and PDF uncertainties at different collider energies. At the 13 TeV LHC, the NLO correction increases the cross section by 34%. The  $aN^2LO$  result surpasses the NLO prediction by 12%. It is important to note that the scale-independent parts of the hard and soft functions contribute one-third of the  $\mathcal{O}(\alpha_s^2)$  corrections. More specifically, 24% (9%) comes from the hard (soft) function. The  $aN^3LO$  correction provides a further improvement of 2% with respect to the  $aN^2LO$  result. The  $aN^3LO$  prediction lies nearly within the scale uncertainty band of the  $aN^2LO$  result, indicating an excellent perturbative convergence. We also investigate the effect of the triple correlation in the three-loop soft function, i.e., the last term in Eq. (5), finding that they give a 5% contribution to the  $\mathcal{O}(\alpha_s^3)$  correction. From this table, one can observe that the PDF uncertainties are around 2%, independent of the perturbative orders. This is because we have used the same PDF set in the calculations at different orders. The results at other collider energies display similar features.

Fig. 3 shows the comparison between theoretical predictions and ATLAS and CMS measurements at  $\sqrt{s}=7$  [3, 8], 8 [6, 9], 13 [7, 12], 13.6 [13] TeV. It can be clearly seen that the central values of the experimental data

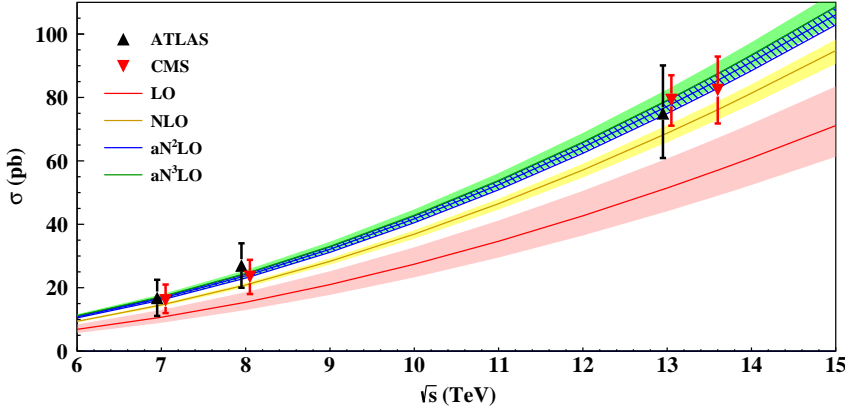


FIG. 3: Comparison between measured cross sections for  $tW^-/\bar{t}W^+$  production at the LHC [3, 6–9, 12, 13] and theoretical predictions. The bands in theoretical predictions denote the scale uncertainties.

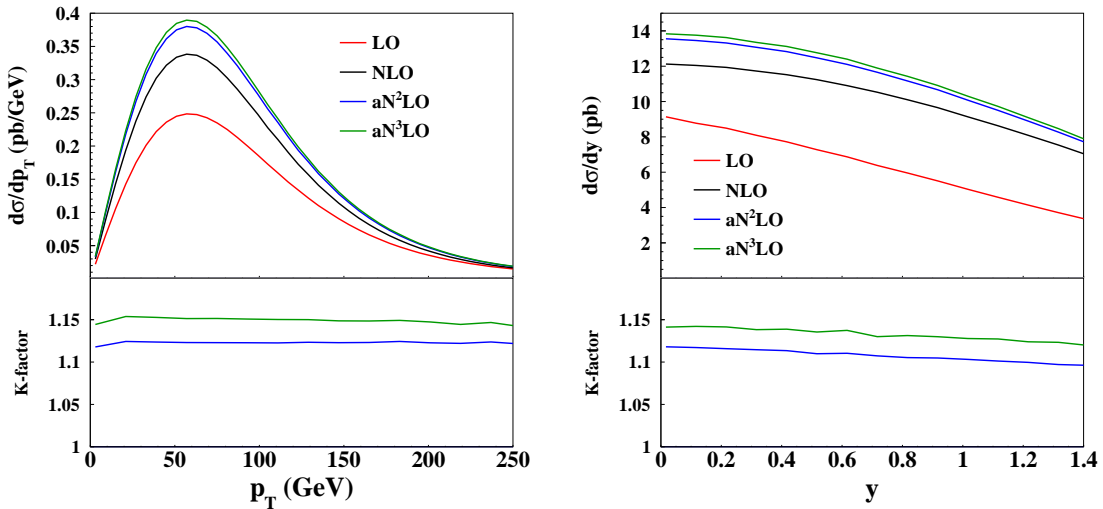


FIG. 4: Top quark  $p_T$  distribution (left) and rapidity distribution (right) at the 14 TeV LHC. The top panels show results at different perturbative orders. The bottom panels show the K-factor as the ratio of the  $aN^2LO$  ( $aN^3LO$ ) over the NLO results.

agree better with the  $aN^2LO$  and  $aN^3LO$  predictions than the NLO ones, underlining the necessity of including higher-order corrections. From this comparison, we can derive the Cabibbo–Kobayashi–Maskawa (CKM) matrix element  $V_{tb}$  directly as the cross section is proportional to  $|V_{tb}|^2$ , given that the processes induced by a strange or down quark are highly suppressed due to the tiny values of the CKM matrix elements  $V_{ts}$  ( $\sim 4 \times 10^{-2}$ ) and  $V_{td}$  ( $\sim 9 \times 10^{-3}$ ) [49]. Consequently, we obtain  $|V_{tb}| = 0.99 \pm 0.03(\text{exp.}) \pm 0.03(\text{theo.})$  where the first and second errors represent the experimental and theoretical uncertainties, respectively. This result, based on measurements of a single process, agrees with the world average value in [49] with comparable accuracy.

Fig. 4 shows the top-quark transverse momentum and

rapidity distributions. The  $aN^2LO$  and  $aN^3LO$  corrections are sizable across the full regions, and thus should be included in the precise predictions. Since their effects have only weak kinematic dependence, it is sufficient to apply a universal K-factor.

#### IV. CONCLUSION

We have calculated the approximate  $N^2LO$  and  $N^3LO$  QCD corrections for  $tW$  associated production at the LHC, which constitute the dominant contributions to the corresponding full perturbative predictions. Our calculation incorporates the  $N^2LO$  hard and soft functions as well as the complete  $N^3LO$  soft anomalous dimension, en-

abling an unprecedented level of precision. These higher-order corrections are found to increase the NLO cross section by more than 10% and lead to improved agreement with experimental data. Consequently, this allows for a direct determination of the CKM matrix element  $|V_{tb}| = 0.99 \pm 0.03(\text{exp.}) \pm 0.03(\text{theo.})$  without assuming unitarity. We also investigate the effect of these approximate higher-order corrections on kinematic distributions and find them to be significant. Collectively, these results underscore the importance of higher-order QCD corrections in  $tW$  production and the necessity of including them in experimental analyses.

Looking forward, a complete N<sup>2</sup>LO calculation will be essential to further reduce theoretical uncertainties. Achieving this will require the development of a robust subtraction scheme for the top-quark-pair interference contribution in the  $tW\bar{b}g$  final state, along with a coherent combination of the double-virtual, virtual-real, and double-real corrections.

## ACKNOWLEDGMENTS

We would like to thank Long-Bin Chen, Liang Dong, Zhao Li and Yefan Wang for collaboration on the computation of the two-loop hard function. We thank Wenbin Qian for useful discussion on the statistical analysis. This work was partly supported by the National Natural Science Foundation of China under grants No. 12275156, No. 12321005 and the Taishan Scholar Foundation of Shandong province (tsqn201909011). The Feynman diagrams were drawn using **TikZ-FeynHand** [50]. The authors gratefully acknowledge the valuable discussions and insights provided by the members of the Collaboration of Precision Testing and New Physics.

## Appendix A: Anomalous Dimensions

The perturbative coefficients of the cusp anomalous dimension read [42]

$$\begin{aligned} \gamma_{\text{cusp}}^{(0)} &= 4, \\ \gamma_{\text{cusp}}^{(1)} &= C_A \left( \frac{268}{9} - \frac{4\pi^2}{3} \right) - \frac{80}{9} T_F n_f, \\ \gamma_{\text{cusp}}^{(2)} &= C_A^2 \left( \frac{490}{3} - \frac{536\pi^2}{27} + \frac{44\pi^4}{45} + \frac{88}{3}\zeta_3 \right) \\ &+ C_A T_F n_f \left( -\frac{1672}{27} + \frac{160\pi^2}{27} - \frac{224}{3}\zeta_3 \right) \\ &+ C_F T_F n_f \left( -\frac{220}{3} + 64\zeta_3 \right) - \frac{64}{27} T_F^2 n_f^2. \end{aligned} \quad (\text{A1})$$

The associating function  $\mathcal{F}_{h2}$  can be found in [36] and given by

$$\mathcal{F}_{h2}(r) = 128(G_{-1,0,0,0} + G_{-1,1,0,0} + G_{1,-1,0,0} - G_{1,0,0,0})$$

$$\begin{aligned} &+ 128(\zeta_2 + \zeta_3)(G_{1,0} - G_{-1,0}) + 96(\zeta_3 + \zeta_4)(G_{-1} - G_1) \\ &+ 128\zeta_2(G_{-2,0} - G_{2,0} + G_{-1,0,0} - G_{1,0,0}) + 256(G_{1,2,0,0} \\ &+ G_{2,0,0,0} - G_{-2,0,0,0} + G_{-1,-2,0,0} - G_{-1,2,0,0} - G_{1,-2,0,0} \\ &- G_{-1,0,0,0,0} + G_{1,0,0,0,0}) + 48(2\zeta_2\zeta_3 + \zeta_5), \end{aligned} \quad (\text{A2})$$

where  $G_{a_1, \dots, a_n} \equiv G(a_1, \dots, a_n; \sqrt{\frac{1-\beta_t^2}{1-\beta_t^2 y^2}})$  and  $G$  is the multiple polylogarithm [51]. The perturbative coefficients of  $\gamma_q$  are given by [43]

$$\begin{aligned} \gamma_q^{(0)} &= -3C_F, \\ \gamma_q^{(1)} &= C_F^2 \left( -\frac{3}{2} + 2\pi^2 - 24\zeta_3 \right) \\ &+ C_A C_F \left( -\frac{961}{54} - \frac{11\pi^2}{6} + 26\zeta_3 \right) \\ &+ C_F T_F n_f \left( \frac{130}{27} + \frac{2\pi^2}{3} \right), \\ \gamma_q^{(2)} &= C_F^3 \left( -\frac{29}{2} - 3\pi^2 - \frac{8\pi^4}{5} - 68\zeta_3 + \frac{16\pi^2}{3}\zeta_3 \right. \\ &\left. + 240\zeta_5 \right) + C_F^2 C_A \left( -\frac{151}{4} + \frac{205\pi^2}{9} + \frac{247\pi^4}{135} \right. \\ &\left. - \frac{844}{3}\zeta_3 - \frac{8\pi^2}{3}\zeta_3 - 120\zeta_5 \right) + C_F C_A^2 \left( -\frac{139345}{2916} \right. \\ &\left. - \frac{7163\pi^2}{486} - \frac{83\pi^4}{90} + \frac{3526}{9}\zeta_3 - \frac{44\pi^2}{9}\zeta_3 - 136\zeta_5 \right) \\ &+ C_F^2 T_F n_f \left( \frac{2953}{27} - \frac{26\pi^2}{9} - \frac{28\pi^4}{27} + \frac{512}{9}\zeta_3 \right) \\ &+ C_F C_A T_F n_f \left( -\frac{17318}{729} + \frac{2594\pi^2}{243} - \frac{1928}{27}\zeta_3 \right. \\ &\left. + \frac{22\pi^4}{45} \right) + C_F T_F^2 n_f^2 \left( \frac{9668}{729} - \frac{40\pi^2}{27} - \frac{32}{27}\zeta_3 \right). \end{aligned} \quad (\text{A3})$$

The perturbative coefficients of  $\gamma_g$  read [43]

$$\begin{aligned} \gamma_g^{(0)} &= -\frac{11}{3}C_A + \frac{4}{3}T_F n_f, \\ \gamma_g^{(1)} &= C_A^2 \left( -\frac{692}{27} + \frac{11\pi^2}{18} + 2\zeta_3 \right) \\ &+ C_A T_F n_f \left( \frac{256}{27} - \frac{2\pi^2}{9} \right) + 4C_F T_F n_f, \\ \gamma_g^{(2)} &= C_A^3 \left( -\frac{97186}{729} + \frac{6109\pi^2}{486} - \frac{319\pi^4}{270} + \frac{122}{3}\zeta_3 \right. \\ &\left. - \frac{20\pi^2}{9}\zeta_3 - 16\zeta_5 \right) + C_A^2 T_F n_f \left( \frac{30715}{729} - \frac{1198\pi^2}{243} \right. \\ &\left. + \frac{82\pi^4}{135} + \frac{712\zeta_3}{27} \right) + C_A C_F T_F n_f \left( \frac{2434}{27} - \frac{2\pi^2}{3} \right. \\ &\left. - \frac{8\pi^4}{45} - \frac{304}{9}\zeta_3 \right) - 2C_F^2 T_F n_f - \frac{44}{9}C_F T_F^2 n_f^2 \\ &+ C_A T_F^2 n_f^2 \left( -\frac{538}{729} + \frac{40\pi^2}{81} - \frac{224}{27}\zeta_3 \right). \end{aligned} \quad (\text{A4})$$

The perturbative coefficients of  $\gamma_Q$  are given by [44]

$$\begin{aligned}\gamma_Q^{(0)} &= -2C_F, \\ \gamma_Q^{(1)} &= C_A C_F \left( -\frac{98}{9} + \frac{2\pi^2}{3} - 4\zeta_3 \right) + \frac{40}{9} C_F T_F n_f, \\ \gamma_Q^{(2)} &= C_F C_A^2 \left( -\frac{343}{9} + \frac{304\pi^2}{27} - \frac{22\pi^4}{45} - \frac{740}{9} \zeta_3 \right. \\ &\quad \left. - \frac{4\pi^2}{3} \zeta_3 + 36\zeta_5 \right) + C_F^2 T_F n_f \left( \frac{110}{3} - 32\zeta_3 \right) \\ &\quad + C_F C_A T_F n_f \left( \frac{356}{27} - \frac{80\pi^2}{27} + \frac{496\zeta_3}{9} \right) + \frac{32}{27} C_F T_F^2 n_f^2.\end{aligned}\tag{A5}$$

The perturbative coefficients of  $\gamma_f^q$  read [39]

$$\begin{aligned}\gamma_f^{q,(0)} &= 3C_F, \\ \gamma_f^{q,(1)} &= C_F^2 \left( \frac{3}{2} - 2\pi^2 + 24\zeta_3 \right) - C_F T_F n_f \left( \frac{2}{3} + \frac{8\pi^2}{9} \right) \\ &\quad + C_A C_F \left( \frac{17}{6} + \frac{22\pi^2}{9} - 12\zeta_3 \right), \\ \gamma_f^{q,(2)} &= C_F^3 \left( \frac{29}{2} + 3\pi^2 + \frac{8\pi^4}{5} + 68\zeta_3 - \frac{16\pi^2}{3} \zeta_3 \right. \\ &\quad \left. - 240\zeta_5 \right) + C_F^2 C_A \left( \frac{151}{4} - \frac{205\pi^2}{9} - \frac{247\pi^4}{135} + \frac{844}{3} \zeta_3 \right. \\ &\quad \left. + \frac{8\pi^2}{3} \zeta_3 + 120\zeta_5 \right) + C_F^2 T_F n_f \left( -46 + \frac{20\pi^2}{9} \right.\end{aligned}$$

$$\begin{aligned}&\quad \left. + \frac{116\pi^4}{135} - \frac{272}{3} \zeta_3 \right) + C_F C_A^2 \left( -\frac{1657}{36} + \frac{2248\pi^2}{81} \right. \\ &\quad \left. - \frac{\pi^4}{18} - \frac{1552}{9} \zeta_3 + 40\zeta_5 \right) + C_F C_A T_F n_f \left( 40 \right. \\ &\quad \left. - \frac{1336\pi^2}{81} + \frac{2\pi^4}{45} + \frac{400}{9} \zeta_3 \right) + C_F T_F^2 n_f^2 \left( -\frac{68}{9} \right. \\ &\quad \left. + \frac{160\pi^2}{81} - \frac{64}{9} \zeta_3 \right).\end{aligned}\tag{A6}$$

The perturbative coefficients of  $\gamma_f^q$  are given by [46]

$$\begin{aligned}\gamma_f^{g,(0)} &= \frac{11}{3} C_A - \frac{4}{3} T_F n_f, \\ \gamma_f^{g,(1)} &= C_A^2 \left( \frac{32}{3} + 12\zeta_3 \right) - \frac{16}{3} C_A T_F n_f - 4C_F T_F n_f, \\ \gamma_f^{g,(2)} &= C_A^3 \left( \frac{79}{2} + \frac{4\pi^2}{9} + \frac{11\pi^4}{54} + \left( \frac{536}{3} - \frac{8\pi^2}{3} \right) \zeta_3 \right. \\ &\quad \left. - 80\zeta_5 \right) - C_A^2 T_F n_f \left( \frac{233}{9} + \frac{8\pi^2}{9} + \frac{2\pi^4}{27} + \frac{160}{3} \zeta_3 \right) \\ &\quad - \frac{241}{9} C_A C_F T_F n_f + 2C_F^2 T_F n_f + \frac{58}{9} C_A T_F^2 n_f^2 \\ &\quad + \frac{44}{9} C_F T_F^2 n_f^2.\end{aligned}\tag{A7}$$

---

[1] J. A. Aguilar-Saavedra, *Nucl. Phys. B* **843**, 638 (2011), [Erratum: Nucl.Phys.B 851, 443–444 (2011)], arXiv:1008.3562 [hep-ph].

[2] C. Zhang and S. Willenbrock, *Phys. Rev. D* **83**, 034006 (2011), arXiv:1008.3869 [hep-ph].

[3] G. Aad *et al.* (ATLAS), *Phys. Lett. B* **716**, 142 (2012), arXiv:1205.5764 [hep-ex].

[4] G. Aad *et al.* (ATLAS), *JHEP* **01**, 064 (2016), arXiv:1510.03752 [hep-ex].

[5] M. Aaboud *et al.* (ATLAS), *JHEP* **01**, 063 (2018), arXiv:1612.07231 [hep-ex].

[6] G. Aad *et al.* (ATLAS), *Eur. Phys. J. C* **81**, 720 (2021), arXiv:2007.01554 [hep-ex].

[7] G. Aad *et al.* (ATLAS), *Phys. Rev. D* **110**, 072010 (2024), arXiv:2407.15594 [hep-ex].

[8] S. Chatrchyan *et al.* (CMS), *Phys. Rev. Lett.* **110**, 022003 (2013), arXiv:1209.3489 [hep-ex].

[9] S. Chatrchyan *et al.* (CMS), *Phys. Rev. Lett.* **112**, 231802 (2014), arXiv:1401.2942 [hep-ex].

[10] A. M. Sirunyan *et al.* (CMS), *JHEP* **10**, 117 (2018), arXiv:1805.07399 [hep-ex].

[11] A. Tumasyan *et al.* (CMS), *JHEP* **11**, 111 (2021), arXiv:2109.01706 [hep-ex].

[12] A. Tumasyan *et al.* (CMS), *JHEP* **07**, 046 (2023), arXiv:2208.00924 [hep-ex].

[13] A. Hayrapetyan *et al.* (CMS), *JHEP* **01**, 107 (2025), arXiv:2409.06444 [hep-ex].

[14] W. T. Giele, S. Keller, and E. Laenen, *Phys. Lett. B* **372**, 141 (1996), arXiv:hep-ph/9511449.

[15] S. Zhu, *Phys. Lett. B* **524**, 283 (2002), [Erratum: Phys.Lett.B 537, 351–352 (2002)], arXiv:hep-ph/0109269.

[16] Q.-H. Cao, (2008), arXiv:0801.1539 [hep-ph].

[17] J. M. Campbell and F. Tramontano, *Nucl. Phys. B* **726**, 109 (2005), arXiv:hep-ph/0506289.

[18] S. Frixione, E. Laenen, P. Motylinski, B. R. Webber, and C. D. White, *JHEP* **07**, 029 (2008), arXiv:0805.3067 [hep-ph].

[19] E. Re, *Eur. Phys. J. C* **71**, 1547 (2011), arXiv:1009.2450 [hep-ph].

[20] T. Ježo, J. M. Lindert, P. Nason, C. Oleari, and S. Pozzorini, *Eur. Phys. J. C* **76**, 691 (2016), arXiv:1607.04538 [hep-ph].

[21] N. Kidonakis, *Phys. Rev. D* **74**, 114012 (2006), arXiv:hep-ph/0609287.

[22] N. Kidonakis, *Phys. Rev. D* **82**, 054018 (2010), arXiv:1005.4451 [hep-ph].

[23] N. Kidonakis, *Phys. Rev. D* **96**, 034014 (2017), arXiv:1612.06426 [hep-ph].

[24] C. S. Li, H. T. Li, D. Y. Shao, and J. Wang, *JHEP* **06**, 125 (2019), arXiv:1903.01646 [hep-ph].

[25] N. Kidonakis and N. Yamanaka, *JHEP* **05**, 278 (2021), arXiv:2102.11300 [hep-ph].

- [26] L.-B. Chen and J. Wang, *Chin. Phys. C* **45**, 123106 (2021), arXiv:2106.12093 [hep-ph].
- [27] M.-M. Long, R.-Y. Zhang, W.-G. Ma, Y. Jiang, L. Han, Z. Li, and S.-S. Wang, (2021), arXiv:2111.14172 [hep-ph].
- [28] J. Wang and Y. Wang, *JHEP* **02**, 127 (2023), arXiv:2211.13713 [hep-ph].
- [29] L.-B. Chen, L. Dong, H. T. Li, Z. Li, J. Wang, and Y. Wang, *JHEP* **08**, 211 (2022), arXiv:2204.13500 [hep-ph].
- [30] L.-B. Chen, L. Dong, H. T. Li, Z. Li, J. Wang, and Y. Wang, *Phys. Rev. D* **106**, 096029 (2022), arXiv:2208.08786 [hep-ph].
- [31] L.-B. Chen, L. Dong, H. T. Li, Z. Li, J. Wang, and Y. Wang, *JHEP* **07**, 089 (2023), arXiv:2212.07190 [hep-ph].
- [32] H. T. Li and J. Wang, *JHEP* **02**, 002 (2017), arXiv:1611.02749 [hep-ph].
- [33] H. T. Li and J. Wang, *Phys. Lett. B* **784**, 397 (2018), arXiv:1804.06358 [hep-ph].
- [34] L. Dong, H. T. Li, Z.-Y. Li, and J. Wang, *JHEP* **01**, 158 (2025), arXiv:2411.07455 [hep-ph].
- [35] J.-L. Ding, H. T. Li, and J. Wang, *JHEP* **05**, 143 (2025), arXiv:2502.18648 [hep-ph].
- [36] Z. L. Liu and N. Schalch, *Phys. Rev. Lett.* **129**, 232001 (2022), arXiv:2207.02864 [hep-ph].
- [37] N. Kidonakis, *Phys. Rev. D* **75**, 071501 (2007), arXiv:hep-ph/0701080.
- [38] N. Kidonakis, *Phys. Rev. D* **99**, 074024 (2019), arXiv:1901.09928 [hep-ph].
- [39] T. Becher, M. Neubert, and G. Xu, *JHEP* **07**, 030 (2008), arXiv:0710.0680 [hep-ph].
- [40] S. Catani and M. H. Seymour, *Phys. Lett. B* **378**, 287 (1996), arXiv:hep-ph/9602277.
- [41] S. Catani and M. H. Seymour, *Nucl. Phys. B* **485**, 291 (1997), [Erratum: Nucl.Phys.B 510, 503–504 (1998)], arXiv:hep-ph/9605323.
- [42] S. Moch, J. A. M. Verma, and A. Vogt, *Nucl. Phys. B* **688**, 101 (2004), arXiv:hep-ph/0403192.
- [43] T. Becher and M. Neubert, *JHEP* **06**, 081 (2009), [Erratum: JHEP 11, 024 (2013)], arXiv:0903.1126 [hep-ph].
- [44] R. Brüser, Z. L. Liu, and M. Stahlhofen, *JHEP* **03**, 071 (2020), arXiv:1911.04494 [hep-ph].
- [45] G. P. Korchemsky and G. Marchesini, *Nucl. Phys. B* **406**, 225 (1993), arXiv:hep-ph/9210281.
- [46] V. Ahrens, T. Becher, M. Neubert, and L. L. Yang, *Eur. Phys. J. C* **62**, 333 (2009), arXiv:0809.4283 [hep-ph].
- [47] R. D. Ball *et al.* (PDF4LHC Working Group), *J. Phys. G* **49**, 080501 (2022), arXiv:2203.05506 [hep-ph].
- [48] A. Buckley, J. Ferrando, S. Lloyd, K. Nordström, B. Page, M. Rüfenacht, M. Schönherr, and G. Watt, *Eur. Phys. J. C* **75**, 132 (2015), arXiv:1412.7420 [hep-ph].
- [49] S. Navas *et al.* (Particle Data Group), *Phys. Rev. D* **110**, 030001 (2024).
- [50] M. Dohse, (2018), arXiv:1802.00689 [cs.OH].
- [51] A. B. Goncharov, arXiv e-prints , arXiv:1105.2076 (2011), arXiv:1105.2076 [math.AG].